AIAA AVIATION Forum
August 2-6, 2021, VIRTUAL EVENT
AIAA AVIATION 2021 FORUM

10.2514/6.2021-2802

A heavy sphere in a vertical jet: A simple pedagogical demonstration of aerodynamics and stability

Zachary Swartzwelder,* Samuel C. Woolsey,*
Blacksburg High School, Blacksburg, VA 24060, USA

Craig A. Woolsey†
Virginia Tech, Blacksburg, VA 24061, USA

The phenomenon of a light-weight sphere floating within a vertical jet illustrates a variety of fundamental concepts in fluid dynamics and rigid body mechanics. The phenomenon is described here in the context of several learning objectives that are revisited throughout the paper. The paper presents fundamental theory, physical analysis, and experimental results that illustrate important concepts such as Bernoulli's principle, fluid dynamic drag, and the existence and stability of equilibria. While the discussion touches on a few advanced topics, such as multivariable calculus and ordinary differential equations, the presentation is largely appropriate to science, technology, engineering, and mathematics (STEM) instruction at the level of a high school upper classman. The paper is targeted toward STEM educators.

I. Introduction

The movement of objects through fluids has been a focus of human inquiry for millennia, culminating in modern disciplines like aerospace engineering and naval architecture. While many questions are still unresolved, ranging from turbulent boundary layer physics to hypersonic combustion, the foundational principles outlined by Euler, Bernoulli, and others remain extremely useful in understanding basic fluid flow and they provide an important gateway for students of the discipline. These basic fluid flows, and the underlying mathematical physics, continue to capture the curiosity of future engineers from an early age.

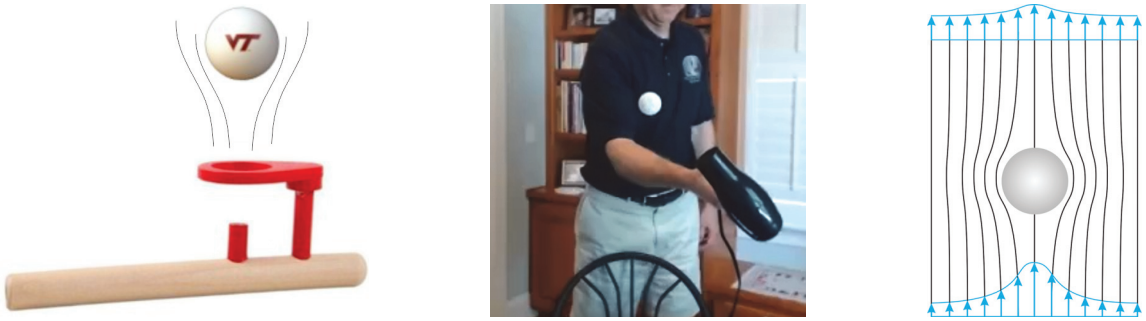

(a) Blow pipe toy (b) Hair dryer and table tennis ball (c) Conceptual sketch

Fig. 1 A heavy sphere in a vertical jet.

Figure 1(a) shows a simple toy – a "blow pipe" and a light-weight sphere – that provides a surprisingly rich example. The principle of the toy's operation is that blowing through the pipe creates an upward vertical jet in which the ball "floats." The phenomenon can also be demonstrated with a hair dryer and a table tennis ball. The fact of this stable equilibrium is surprising enough, to those who have not observed it before, but its robustness to disturbances is even more striking. One may tilt the flow substantially while sustaining the equilibrium, as illustrated in Figure 1(b). While an expert would immediately recognize a number of subtle complexities, a simple analysis can go far in explaining the existence and stability of the equilibrium.

*Student, Blacksburg High School
†Professor, Kevin T. Crofton Department of Aerospace and Ocean Engineering, AIAA Associate Fellow

This brief paper summarizes the physics underlying the several phenomena illustrated in Figure 1 at a level that is accessible to high school STEM educators. We start by briefly describing the target audience for this educational module, both the instructors and the students, and then we present a number of relevant learning objectives. We then provide a brief discussion of the underlying physics, including Bernoulli's principle, friction and pressure drag, and the general character of laminar and turbulent cylindrical jets. We then use these concepts to qualitatively explain the phenomenon in which a heavy sphere remains suspended in an upward vertical jet. For readers with a background in differential equations, we also include an analytical treatment of the problem in terms of a cylindrical laminar jet and a sphere that is small relative to the scale of flow variations. Next, we describe a set of experiments which allow a comparison with this simplified analytical treatment. aimed at quantifying elements of the qualitative description. Specifically, we measure the flow field emanating from a hair dryer (with the heating element disabled) using a Pitot-static probe. We then use video image analysis to determine the equilibrium height of a number of light-weight spheres that are released into this vertical jet. Finally, we briefly discuss the spheres' motion in response to small disturbances and the concept of stability of equilibria.

II. Learning Objectives

The aim of this paper is to provide a brief physics tutorial to supplement classroom demonstrations of a heavy sphere in vertical jet. The target audience is a high school STEM educator whose students have taken courses in algebra and physics. A student with some exposure to calculus-based physics will better appreciate the discussion of stability, but that is certainly not required. Following are five learning objectives that are supported by the material in this paper.

- State Bernoulli's principle for steady, incompressible, inviscid flow and describe its implications.
- Compute a flow velocity from pressure measurements obtained using a Pitot-static probe.
- Describe the qualitative nature of a steady, laminar jet and a turbulent jet.
- Explain the drag force acting on a sphere immersed in a steady, incompressible, viscous flow.
- Describe the notions of equilibrium and stability, in general terms.
- Describe the nature of the equilibrium in which a heavy sphere is supported by a vertical jet, including the physical mechanisms that make this equilibrium stable.

The following section describes the underlying physics that support these student learning objectives.

III. Underlying Physics

The physics of a heavy sphere levitating in a vertical jet is well studied as a topic of fundamental research [1, 2] as well as as an engaging example for physics education [3–5]. The existence and stability of the equilibrium is typically attributed to the *Coanda effect* which describes the interaction between the flow and the solid sphere [1–3]. However, a simpler model that ignores the effect of the sphere on the flow field admits a qualitatively similar behavior [4]. Adopting this simpler perspective, we assume the heavy sphere experiences a drag force commensurate with its size, but does not affect the surrounding flow field. One aim of the experimental effort is to evaluate the merit of this simplifying assumption.

In considering the flow produced by a blow pipe or a hair dryer, we make several other simplifying assumptions:

- the air density remains constant (i.e., the flow is *incompressible*),
- the flow is "frictionless" (i.e., the fluid is *inviscid*), and
- the air velocity at any point is constant (i.e., the flow is *steady*).

The first of these assumptions is the least objectionable. Compressibility becomes an issue only when a flow approaches the speed of sound in the given fluid – about 344 m/s for air in standard, sea level conditions [6].

The second assumption seems restrictive, since any real fluid is "sticky," but the approximation is often quite accurate, except within a thin layer near the walls of immersed objects and within the resulting wake – concepts that will be revisited shortly.

For the experiment considered here, the third assumption is reasonable in regions where the second assumption holds, provided the heavy sphere remains in equilibrium. If the sphere is perturbed from its equilibrium, then its position and the surrounding flow evolve interdependently until the sphere either escapes or settles back to its equilibrium. As we've said above, however, we will assume the flow field is unaffected by motion of the sphere so that the flow remains steady.

A. Bernoulli's principle

Figure 1(c) depicts an upward vertical jet and a heavy sphere suspended at rest in the flow. We will discuss the conditions under which this arrangement is feasible shortly. For now, we assume the sphere is held in place by some invisible means. To illustrate the flow, Figure 1(c) depicts several *streamlines* – curves that are everywhere tangent to the local flow velocity. Under the stated assumptions of steady, inviscid, incompressible flow, each of these streamlines enjoys a special property expressed by *Bernoulli's equation* [7, Ch. 3]:

$$P_{\text{total}} = P + \frac{1}{2}\rho V^2 + \rho g z = \text{constant along a streamline} \tag{1}$$

The term P is the *static pressure* – the pressure one would measure when moving along the streamline at the flow velocity, so that the surrounding fluid is "static" relative to the moving sensor. The term $\frac{1}{2}\rho V^2$ is the *dynamic pressure* associated with the fluid motion. Here ρ is the fluid density and V is the flow speed. While this term has units of pressure, it is really a measure of kinetic energy. In fact, Bernoulli's equation may be interpreted as an energy conservation law. In this interpretation, the term $\rho g z$ in equation (1) accounts for gravitational potential energy. The conservation law indicates that as a streamline gains height z above some datum, the sum of static and dynamic pressure must decrease so that the total pressure P_{total} remains constant. Conversely, as a streamline's height decreases, the sum of static and dynamic pressure must increase. For the vertical jet considered here, we assume that the variations in this third term are negligible compared with the first two.

The first two terms in (1) sum to form the *stagnation pressure*. Considering a flow in which the gravitational term can be neglected, such as a purely horizontal flow, the stagnation pressure is the pressure one would measure by placing a pressure sensor normal to a streamline so that the flow is forced to "stagnate" at the sensor. By combining independent measurements of the static pressure and the stagnation pressure at nearby points in a flow, one may determine the dynamic pressure. If the fluid density is known, one may then extract the airspeed, a concept that is the basis for the most common airspeed measurement device: the Pitot-static probe.

Bernoulli's equation (1) applies along a streamline. However, the total pressure P_{total} is not necessarily the same across streamlines. If one adopts a fourth assumption – that the flow is *irrotational* – then the total pressure is constant across streamlines. The formal definition of an irrotational flow involves vector calculus, but the basic notion is that small parcels of fluid do not spin as they move along streamlines. While many natural flows can be considered irrotational, the assumption is not appropriate for a vertical jet.

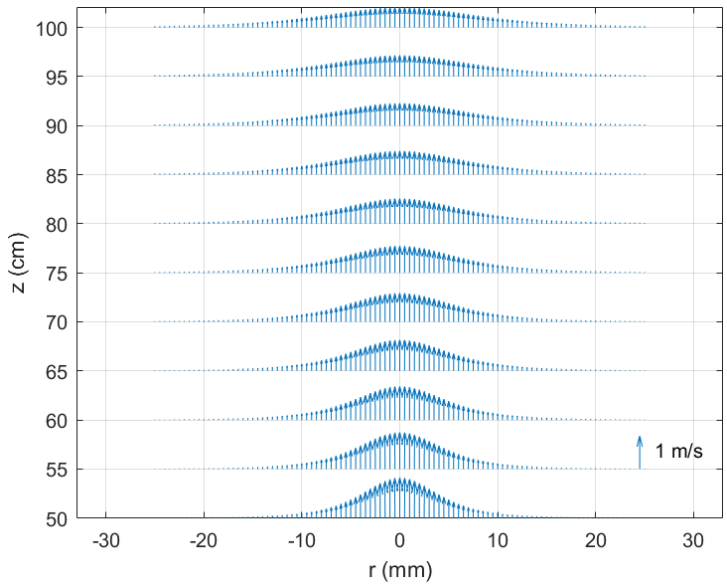

(a) Example of an axisymmetric laminar jet.

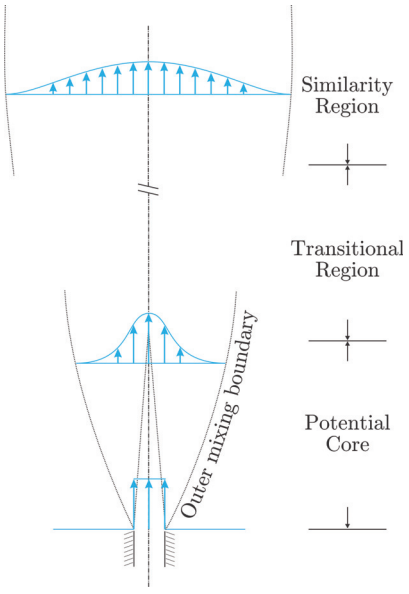

(b) Structure of a turbulent jet, after [8].

Fig. 2 Axisymmetric jets.

B. Laminar and turbulent jets

While the differential equations that describe the flow of a viscous fluid are well known, there are relatively few known solutions to these equations. One of these few, attributed by White [9, Sec. 4.10-6] to H. Schlichting, corresponds to the "laminar flow of a narrow, axisymmetric jet." In this flow, a jet emanates from a circular orifice in a flat wall into a plenum. Because of viscosity, the jet entrains the surrounding fluid as it penetrates into the volume. Figure 2(a) shows a cross-section of the flow pattern, for a jet of particular strength. The flow is called *axisymmetric* because this flow pattern is the same in every radial direction from a perpendicular axis through the center of the orifice. In Figure 2(a), r represents radial displacement from the axis of symmetry and z represents height above the orifice. While the figure depicts flow velocities, one can imagine the streamlines defined by these velocities. Each streamline belongs to a family of all the streamlines at the given radius. Together, these form a "streamtube" obtained by revolving one streamline about the symmetry axis. The flow is called *laminar* because adjacent streamtubes slide over one another in sheets, like a deck of cards. ("Lamina" is the Latin word for "sheet.")

While it may be possible to generate a laminar jet of the sort described above in practice, the flow emanating from a blow pipe or hair dryer is *turbulent*, with parcels of air churning and mixing in ways that cannot be described using streamlines. Even in this case, though, the axisymmetric jet has a consistent character that can be described qualitatively by the *time-averaged* behavior of these air parcels. Moreover, while the notion of streamlines is inappropriate for a turbulent flow, it can be helpful in understanding the time-averaged flow.

Discussing the case of an axisymmetric jet in an ambient stream moving parallel to the axis of symmetry, Schetz [8, Ch.II] describes the evolution of the jet in terms of three regions. Nearest the source is a *potential core* of essentially inviscid flow. Next, in an intermediate region termed the *transitional region*, viscous shearing between the jet and the ambient fluid causes the two to mix. Finally, much farther downstream, a *similarity region* emerges in which the non-dimensionalized shape of the velocity profile remains constant (although the dimensional profile continues to evolve with increasing distance from the source).

For the low-cost experimental apparatus used here (a hair dryer), the jet is turbulent and is not axisymmetric, with a significant element of "swirl" and some misalignment relative to the hair dryer's cylindrical duct. Regardless, to simplify analysis, we assume the time-averaged flow is axisymmetric.

C. Friction and pressure drag

Though we will ignore the effect of the sphere on the jet, it is still necessary to consider the nature of fluid flow around a sphere. The steady flow of an inviscid, constant-density fluid over a sphere can be described by the behavior of nearby streamlines. We neglect gravitational effects and begin by considering an irrotational flow that is initially uniform, as depicted at the left side of Figure 3(a), so that the total pressure is constant across streamlines.

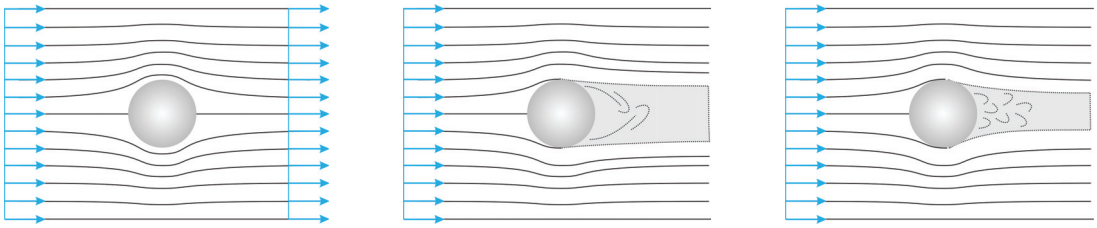

(a) Inviscid flow (b) Viscous flow: Subcritical Re (c) Viscous flow: Supercritical Re

Fig. 3 A sphere in uniform, horizontal flow.

Disallowing the mathematical possibility of discontinuities in the flow field [10, Ch. 1, § 9], the distinguishing characteristic of the flow over the sphere is the "stagnation streamline" which comes to rest on the windward and leeward sides of the sphere. Nearby streamlines hug the sphere while more distant streamlines exhibit smaller deviations from their initial direction.

From Bernoulli's equation, one infers that the static pressure P within the flow field is greatest at the windward and leeward *stagnation points* where it is equal to the total pressure P_{total}. The static pressure is smallest along the diameter of the bisecting plane, where streamlines have been "squeezed" together by the presence of the sphere. At these locations, the flow velocity is faster than anywhere else – faster even than the free stream velocity far upstream. The fact that the flow is symmetrical on the windward and leeward sides of the sphere implies that the force of pressure cancels

over the surface. The absence of a drag force in these idealized conditions is referred to as d'Alembert's paradox [11].

For a sphere immersed in a flow of real fluid, the situation is quite different. Consider again the case of a uniform, incompressible flow, but now suppose the fluid is viscous. Real fluids stick to solid objects – the "no-slip" condition. For a sphere immersed in a real fluid flow, the fluid velocity transitions from zero at the surface of the sphere to the nonzero ambient velocity with increasing distance from the surface. This thin transition region between the object's surface and the ambient flow is called the *boundary layer*. The nature of this process is characterized by the nondimensional *Reynolds number*:

$$\mathrm{Re} = \frac{\rho V L}{\mu}$$

Here, L is a characteristic length (e.g., the diameter of the sphere) and μ is the fluid viscosity, a positive parameter value that characterizes the fluid's "stickiness." (For air at standard sea level conditions, $\mu = 1.789 \times 10^{-5}$ kg/(m s).) For the experiment described here, the Reynolds number based on diameter is on the order of 10^4. In this case, the flow over the windward side of the sphere is reasonably well characterized by the ideal flow scenario described above, except within the boundary layer near the sphere's surface. The ambient flow accelerates around the windward half of the sphere, as before, but as it approaches the maximum diameter a new phenomenon arises which dominates the rest of the flow near the object: the thin boundary layer reverses direction near the wall of the sphere, causing this layer to peel away from the surface and generating a chaotic wake of randomly moving fluid downstream. For a smooth sphere in a flow for which Re is between about 10^3 and 10^5, this wake is relatively large, as in Figure 3(b). As Re increases, there is a sudden and dramatic change in the nature of the flow. The exact value of Re at which this happens – the *critical* Reynolds number alluded to in Figure 3 – is sensitive to the flow conditions, but for $\mathrm{Re} > 10^6$, one sees a much narrower wake [7, Ch. 9], as in Figure 3(c).

A sphere in a uniform flow of real fluid experiences a drag force in the direction of the flow. This force has two sources: friction and pressure. The contribution of friction to the drag force $\mathcal{D}$ on the sphere arises from the stickiness of the fluid – the fluid exerts a shearing force, tugging on the surface of the sphere as it flows around. The contribution of pressure to the drag on the sphere arises from the wake created by the boundary layer's separation from the surface. The pressure within this wake is lower than it would be if the flow were inviscid. So while the sphere experiences a region of high pressure on its windward side, especially in the vicinity of the stagnation point, this same high pressure is not recovered on the leeward side as it was in the case illustrated in Figure 3(a). The result is that the force of pressure no longer cancels over the surface; there is a net pressure force in the direction of the flow. The balance of contributions to the drag force $\mathcal{D}$ from friction and pressure vary with the character of the flow, but the net effect is captured by the following expression:

$$\mathcal{D} = C_D(\mathrm{Re}) \left(\frac{1}{2} \rho V^2 \right) S$$

The parameter $C_D(\mathrm{Re})$ is the nondimensional *drag coefficient* which is a function of the Reynolds number, as indicated, as well as the object's shape and finish. The drag coefficient for a smooth sphere, referenced to the frontal area $S = \frac{1}{4}\pi D^2$, is shown in Figure 4. Note the "drag crisis" that occurs at the critical Reynolds number $\mathrm{Re} = 350,000$. In the Reynolds number range of our experiments, $C_D \approx 0.5$.

The discussion above concerns a sphere in a uniform flow. While it is important that the vertical jet is *nonuniform*, the phenomena described above are qualitatively similar for the experiment we consider. As described next, the drag force due to friction and pressure on the sphere balances the weight of the sphere to establish the equilibrium state.

D. Existence of equilibria

We consider a heavy sphere of mass m and diameter D immersed in an upward vertical jet. (We ignore the effect of gravity on this flow.) Assuming the jet is axisymmetric, we ignore azimuthal motion about the axis of symmetry and consider only the radial and vertical motion of the sphere.

The air velocity within the vertical jet can be decomposed into a radial component $v(r, z)$ and an upward vertical component $w(r, z)$. We assume the flow is *steady* so that these velocity components do not vary with time. Also, as explained earlier, we ignore the fact that the flow field velocity is affected by the presence and motion of the sphere.

The equations describing the sphere's motion follow from Newton's second law:

$$m \frac{d^2 r}{dr^2} = F_r(r, z) \qquad \text{and} \qquad m \frac{d^2 z}{dt^2} = F_z(r, z)$$

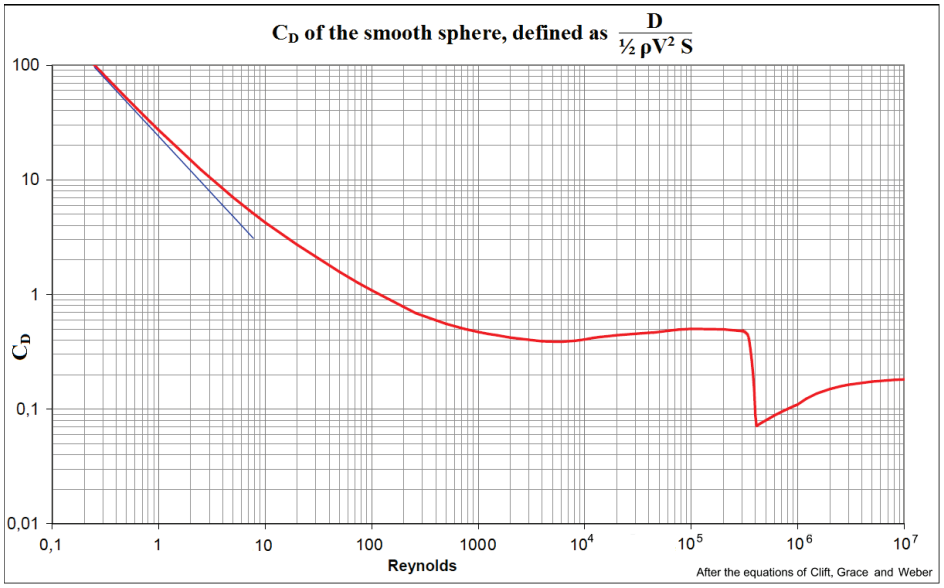

Fig. 4 Drag coefficient on a smooth sphere [12].

where F_r and F_z represent the total force acting on the sphere in the radial and upward directions, respectively. An *equilibrium* is a pair of constant values $r(t) = r_{\text{eq}}$ and $z(t) = z_{\text{eq}}$ which satisfy the equations above:

$$0 = F_r(z_{\text{eq}}, r_{\text{eq}}) \qquad \text{and} \qquad 0 = F_z(z_{\text{eq}}, r_{\text{eq}})$$

To find equilibria, we must know the functional forms of F_r and F_z. But by considering axial symmetry we may immediately conclude that the radial flow velocity v and the radial force F_r must vanish when the sphere is centered along the symmetry axis: $v(0, z) = 0$ and $F_r(0, z) = 0$. We seek equilibria for which $r = r_{\text{eq}} = 0$.

Let v_{r} and w_{r} denote the velocity of the sphere relative to the local airflow:

$$v_{\text{r}}(r, z) = \dot{r} - v(r, z) \qquad \text{and} \qquad w_{\text{r}}(r, z) = \dot{z} - w(r, z)$$

(The roman subscript "r" denotes "relative" while the italic subscript "r" denotes "radial.") We also define the total velocity of the sphere relative to the airflow:

$$V_{\text{r}}(r, z) = \sqrt{v_{\text{r}}(r, z)^2 + w_{\text{r}}(r, z)^2}$$

If the sphere is at rest at some location $(r_{\text{eq}}, z_{\text{eq}}) = (0, z_{\text{eq}})$, we have

$$v_{\text{r}}(0, z_{\text{eq}}) = -v(0, z_{\text{eq}}) = 0 \qquad \text{and} \qquad w_{\text{r}}(0, z_{\text{eq}}) = -w(0, z_{\text{eq}})$$

For this state to be an equilibrium, the force acting on the sphere in the vertical direction must vanish [13]:

$$F_z(0, z_{\text{eq}}) = 0 = -mg + C_D \frac{1}{2} \rho V_{\text{r}}(0, z_{\text{eq}})^2 S - \left. \frac{\partial w}{\partial z} \right|_{(0, z_{\text{eq}})} \tag{2}$$

The first term on the right is the weight of the sphere, acting down. The second term is the drag on the sphere, acting up. The third term is a bit less intuitive; it is a consequence of the *nonuniformity* of the flow field in the vertical direction. This nonuniformity, illustrated by the variation in flow field velocity seen in Figure 2, plays an important role in the *stability* of the equilibrium.

As an example, we will consider the laminar jet mentioned in Section III.B and illustrated in Figure 2(a). As described in [9], the component velocities for this flow field are

$$w(r, z) = \frac{\nu}{r} F'(\eta) \qquad \text{and} \qquad v(r, z) = \frac{\nu}{r} (\eta F'(\eta) - F(\eta))$$

where $\eta = r/z$ and the *kinematic* viscosity $\nu = \mu/\rho$ consolidates a bit of notation. The dimensionless function $F(\eta)$ and its derivative are

$$F(\eta) = \frac{(C\eta)^2}{1 + \frac{1}{4}(C\eta)^2} \qquad \text{and} \qquad F'(\eta) = \frac{2C^2\eta}{(1 + \frac{1}{4}(C\eta)^2)^2}$$

where the dimensionless constant C characterizes the jet's strength. Given these explicit expressions for the flow velocity as a function of position, one may solve equation (2) explicitly for the equilibrium height z_{eq}. Solutions are the real-valued roots of the cubic polynomial

$$\left(\frac{mg}{2C^4\nu^2}\right) z^3 - \rho C_D S z + 2m \tag{3}$$

To make the example more concrete, we adopt the following parameter values

$$C = 138, \quad \rho = 1.225\ \text{kg/m}^3, \quad \nu = 1.6 \times 10^{-5}\ \text{m}^2/\text{s}, \quad g = 9.81\ \text{m/s}^2, \quad m = 0.001\ \text{kg}, \quad S = 0.05\ \text{m}^2, \quad C_D = 0.5$$

These jet parameters correspond to Figure 2(a). We note that the frontal area S corresponds to a diameter of about 25 cm, which badly violates our assumption of a small sphere that has a negligible effect on the narrow jet. Forgiving this absurdity, one obtains an equilibrium height $z_{\text{eq}} = 71.8$ cm. We next consider the stability of this equilibrium.

E. Stability of equilibria

Referring to Figure 2(a), one can see that over the range of heights that are shown the flow velocity decreases with increasing height. As a result, a small upward displacement of the sphere from its equilibrium height z_{eq} will result in a smaller drag force. The upward drag will then fail to balance the weight and the sphere will fall downward. (The gradient term in 2 also changes, but we defer the discussion of that term for a bit.) Conversely, a small downward displacement of the sphere will cause a larger drag force, which would lift the sphere upward. Because these small static displacements result in forces that tend (initially, at least) to restore the equilibrium, we call the equilibrium *statically stable* in the vertical direction.

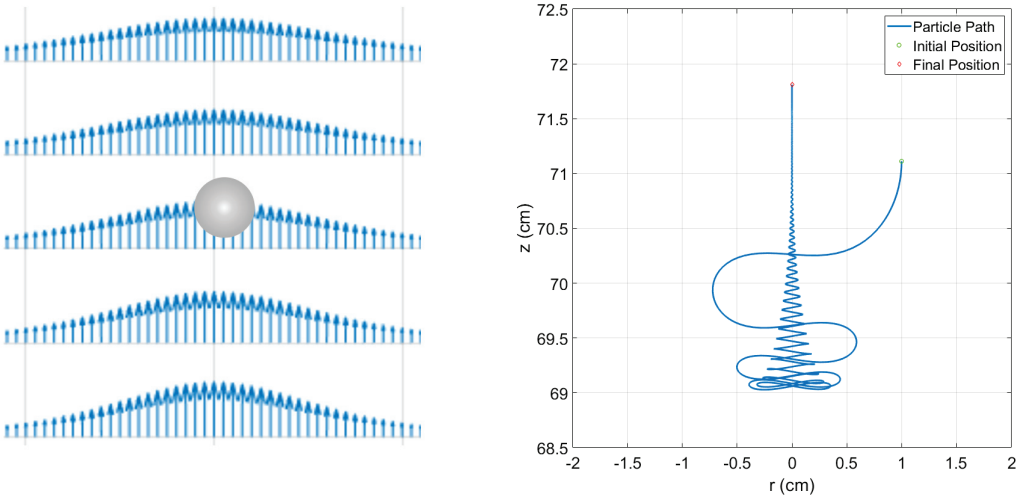

(a) An offset sphere in a cylindrical laminar jet.

(b) Path of the sphere after perturbation.

Fig. 5 Simulation results illustrating stability of the equilibrium.

To establish static stability in the radial direction, we consider another thought experiment, but one which involves Bernoulli's principle. Referring to Figure 5(a), which shows a portion of the flow in Figure 2(a), we imagine a sphere that has been perturbed radially (to the right) by a small amount. Ignoring the effect of the sphere on the flow field, we can see that the flow over the left side of the sphere in this new, displaced location will be faster than the flow over the right side. If the total pressure was the same for each streamline, we could immediately conclude from Bernoulli's principle that the lower pressure (higher flow velocity) on the left side of the sphere, combined with the higher pressure

(lower flow velocity) on the right side of the sphere would result in a net force to the left. That is, the result of the small perturbation to the right would be an aerodynamic force to the left (a "lift" force, in fact). The same argument would hold for displacements in any radial direction, showing that the equilibrium along the axis of symmetry is statically stable in the radial direction as well as the vertical direction.

The fact that the flow in a laminar jet is irrotational means the total pressure is not the same across streamlines. However, the total pressure is greatest along the centerline and decreases monotonically with increasing radial distance. So the restoring effect of pressure in the radial direction is even stronger.

A more formal stability analysis requires some familiarity with ordinary differential equations. A similar analysis was given in [13, §IV] for an infinite cylinder in a plane, laminar jet. Following that analysis, we develop the two degree of freedom dynamic equations for a sphere in an axisymmetric laminar jet. Again, we assume the sphere does not affect the flow of the jet and, as in [13], we neglect the fact that the flow is rotational.*

Under the given assumptions, a system of ordinary differential equations that serve as a dynamic model for the motion of the sphere in response to small perturbations Δ from an equilibrium is

$$\begin{pmatrix} \Delta\dot{r} \\ \Delta\dot{z} \\ \Delta\dot{v}_\mathrm{r} \\ \Delta\dot{w}_\mathrm{r} \end{pmatrix} = \underbrace{\begin{pmatrix} \boldsymbol{\Phi}_\mathrm{eq}^T & \mathbb{I} \\ -w_{\mathrm{r}_\mathrm{eq}}\boldsymbol{H}_\mathrm{eq} & \frac{1}{m}\rho S C_D w_{\mathrm{r}_\mathrm{eq}}\mathbb{I} - \boldsymbol{\Phi}_\mathrm{eq} \end{pmatrix}}_{\boldsymbol{A}} \begin{pmatrix} \Delta r \\ \Delta z \\ \Delta v_\mathrm{r} \\ \Delta w_\mathrm{r} \end{pmatrix} \tag{4}$$

where, in the notation of [13], $\mathbb{I}$ represents the 2×2 identify matrix, $\boldsymbol{\Phi}_\mathrm{eq}$ represents the flow gradient matrix

$$\boldsymbol{\Phi}_\mathrm{eq} = \begin{pmatrix} \frac{\partial v}{\partial r} & \frac{\partial v}{\partial z} \\ \frac{\partial w}{\partial r} & \frac{\partial w}{\partial z} \end{pmatrix}_\mathrm{eq} = \frac{\nu C^2}{z_\mathrm{eq}^2} \begin{pmatrix} 1 & 0 \\ 0 & -2 \end{pmatrix}$$

and $\boldsymbol{H}_\mathrm{eq}$ represents the Hessian of the vertical velocity component $w(r, z)$

$$\boldsymbol{H}_\mathrm{eq} = \begin{pmatrix} \frac{\partial^2 w}{\partial r^2} & \frac{\partial^2 w}{\partial r \partial z} \\ \frac{\partial^2 w}{\partial r \partial z} & \frac{\partial^2 w}{\partial z^2} \end{pmatrix}_\mathrm{eq} = \frac{2\nu C^4}{z_\mathrm{eq}^3} \begin{pmatrix} -1 & 0 \\ 0 & 2 \end{pmatrix}$$

Here and elsewhere, the subscript "eq" indicates that functions have been evaluated at the equilibrium condition $(r, z) = (0, z_\mathrm{eq})$. Note that $w_{\mathrm{r}_\mathrm{eq}} = -w_\mathrm{eq}$, since the sphere is moving downward relative to the air.

Examining the state matrix $\boldsymbol{A}$ in equation (4), one finds that the linearized dynamics decouple into radial and vertical modes. The characteristic polynomial is

$$\det(\lambda\mathbb{I} - \boldsymbol{A}) = \left(\lambda^2 + b_r\lambda + c_r\right)\left(\lambda^2 + b_z\lambda + c_z\right) \tag{5}$$

where

$$b_r = \left(\frac{\nu C^2}{z_\mathrm{eq}}\right)\frac{2}{m}\rho S C_D \qquad c_r = \left(\frac{\nu^2 C^4}{z_\mathrm{eq}^3}\right)\left[\left(4C^2 - 1\right)\frac{1}{z_\mathrm{eq}} - \frac{2}{m}\rho S C_D\right]$$

$$b_z = \left(\frac{\nu C^2}{z_\mathrm{eq}}\right)\frac{2}{m}\rho S C_D \qquad c_z = 4\left(\frac{\nu^2 C^4}{z_\mathrm{eq}^3}\right)\left[3C^2\frac{1}{z_\mathrm{eq}} - \frac{2}{m}\rho S C_D\right]$$

For the specific equilibrium being considered here, the polynomial (5) has two complex conjugate pairs of roots, corresponding to underdamped oscillatory modes in the radial and vertical directions. It follows that the equilibrium of interest is not only statically stable, but *dynamically stable*. In response to a small perturbation, the sphere converges to the equilibrium asymptotically in time.

Rewriting (5) in terms of the natural frequencies and damping ratios of these modes of motion gives

$$\left(\lambda^2 + 2\zeta_r\omega_{\mathrm{n}_r}\lambda + \omega_{\mathrm{n}_r}^2\right)\left(\lambda^2 + 2\zeta_z\omega_{\mathrm{n}_z}\lambda + \omega_{\mathrm{n}_z}^2\right) \tag{6}$$

For the given parameter values

$$\omega_{\mathrm{n}_r} = 163 \text{ rad/s}, \qquad \zeta_r = 3.9 \times 10^{-5}, \qquad \omega_{\mathrm{n}_z} = 282 \text{ rad/s}, \qquad \zeta_z = 2.3 \times 10^{-5}$$

*Unlike the example in [13], we ignore the effect of added mass. Because the density of air is several orders of magnitude smaller than the density of the sphere, this effect is negligible.

IV. Experiment and Results

Demonstrating the existence and stability of an equilibrium for a heavy sphere in a vertical jet requires only a hair dryer and a table tennis ball. In order to explore a bit further, we developed an experimental program that involved first characterizing the flow field using a Pitot-static probe and then recording and analyzing video footage of spheres of various weight and diameter floating within this flow field.

A. The Pitot-static probe

Figure 6 shows the experimental hardware used to characterize the jet (left) and the experimental setup (right). The Pitot-static probe generates an analog voltage that is fed into an analog-to-digital converter (ADC) port on an Arduino Uno microcontroller; see Figure 6(a). Because the probe is designed to operate over a much larger range of speeds than occur within the jet, an analog circuit was designed to bias and scale the signal in order to obtain greater measurement resolution from the 10-bit ADC. The sensor was then calibrated using the liquid level approach described in [14]. Calibration indicated a clear linear relationship between ADC counts and pressure, although the calibration process is susceptible to bias which creates an unknown shift in the dynamic pressure measurements.

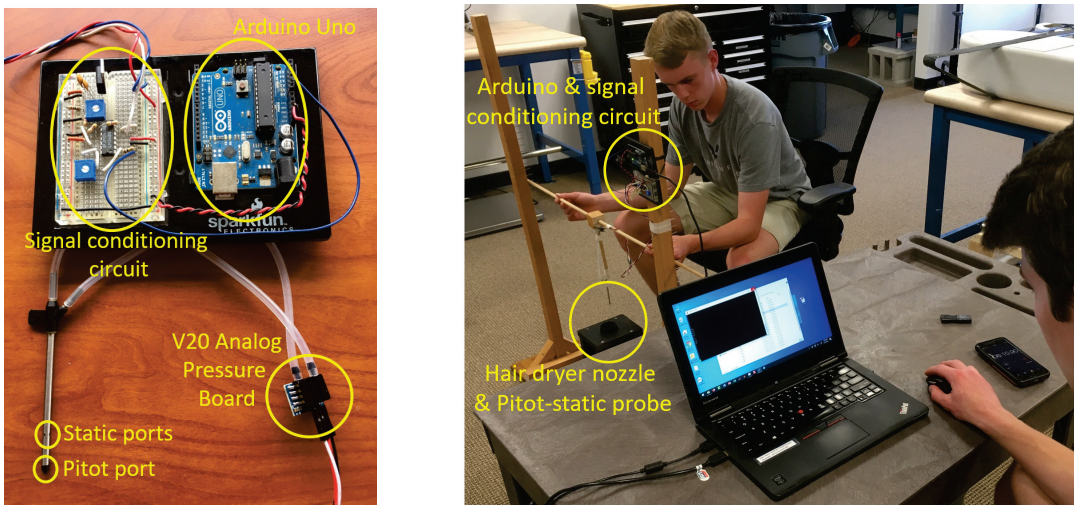

(a) Experimental hardware (b) Experimental setup

Fig. 6 Experimental hardware and setup.

B. Characterizing the flow field

The experimental setup is shown in the annotated photograph in Figure 6(b). A hair dryer, with its heating element disabled, was mounted to generate a vertical flow using one of two power settings: low and high. The vertical component of flow velocity was measured using the Pitot-static probe described in Section IV.A at 15 different heights, measured in 2 cm increments from 2 cm above the exit of the 5 cm diameter nozzle, and at 6 different radial displacements, measured in 1 cm increments from the symmetry axis, inclusive. Dynamic pressure was measured at a sample frequency of 10 Hz for 10 seconds and the data were then averaged. These averaged dynamic pressures were then converted into "equivalent airspeed" measurements using the standard sea level air density of 1.225 kg/m^2. The resulting ("equivalent") flow velocities are reported for the low and high settings in Tables 2 and 3, respectively, in Appendix A. These data are also illustrated in Figures 7(a) and 7(b). The maximum vertical velocity quoted in the caption occurs on the symmetry axis, 2 cm above the nozzle; all vectors in the figure are scaled accordingly. The flow field plots reflect the assumption that the flow is axially symmetric. Note the qualitative similarity with Figure 2.

The setup and instrumentation introduced several sources of error. First, there were obvious variations in flow velocity, especially near the center line of the jet where relative standard deviations in dynamic pressure measurements were in the neighborhood of 40%. These and other issues are revisited in the conclusions in Section V.

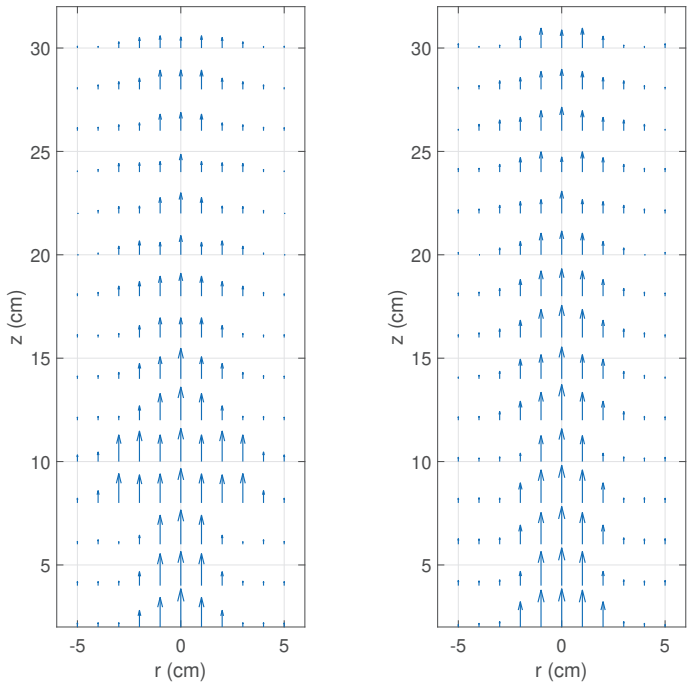

(a) Low: $w_{\max}$ = 15.9 m/s (b) High: $w_{\max}$ = 17.7 m/s

Fig. 7 Symmetrized visualization of average vertical flow velocity.

C. Characterizing equilibria and stability

After characterizing the flow field at the low and high settings, weighted spheres were released into the flow. Four spheres of different diameters and weights were used; see Figure 8. Three of these spheres were dense styrofoam balls with small tungsten weights inserted to increase the mass. The fourth sphere was a table tennis ball.

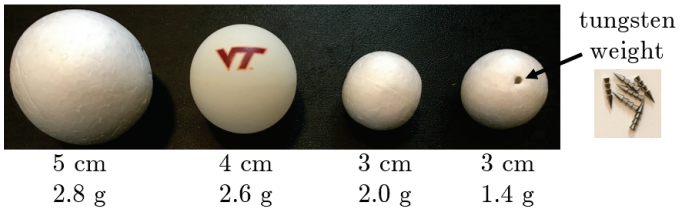

Fig. 8 Test articles, annotated with diameter and mass.

The motion of the spheres was recorded in video which was then analyzed using a Matlab script available from MathWorks [15]. A screenshot of the output from the Matlab script is shown in Figure 9. The screenshot shows an array of images, with the top left being a frame from the raw video footage. The three figures to its right show decompositions into the hue/saturation/value (HSV) color space, with histrograms of the respective parameters aligned below each image. The black and white image at the bottom left is the result of selecting particular HSV threshold values. The image at the far left of the middle row is the original image, annotated with the bounding box and center of mass (in pixels) for each region whose HSV parameter values lie within user-specified bounds.

For the larger two spheres, three phases of motion were analyzed:

- Equilibrium motion.
- Response to a lateral (radial) perturbation.
- Response to a vertical perturbation.

For the lighter 3 cm sphere, the equilibrium was not robust enough to survive intentional perturbations. In fact, the term "equilibrium" must be qualified. None of the four spheres was ever completely at rest within the flow field. In any case, average "equilibrium" heights were obtained from video imagery for all four spheres, as given in Table 1.

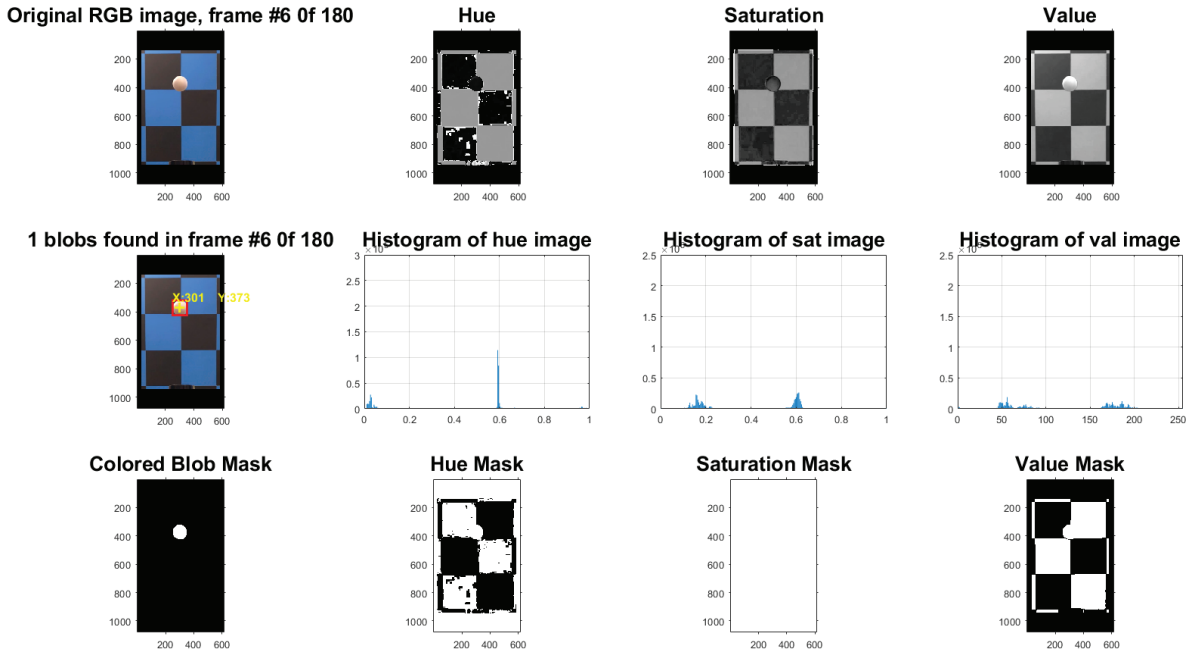

Fig. 9 Screenshot of image frame analysis using the Matlab script `track_color_in_video.m` [15].

Figure 10 shows the position history obtained from a single camera for the 5 cm sphere during a period of undisturbed motion for the high flow setting. Data from the second camera (not shown) account for the out of plane motion. The position indicated in the plot is relative to a reference frame fixed at the center of the nozzle's exit. Several assumptions were made in converting pixel coordinates to physical position. First, it was assumed that the camera is a "pinhole" so that the sphere's position can be reconstructed using a background grid pattern of known geometry. Second, it was assumed that the center of mass extracted from video imagery corresponds to the true center of the sphere.

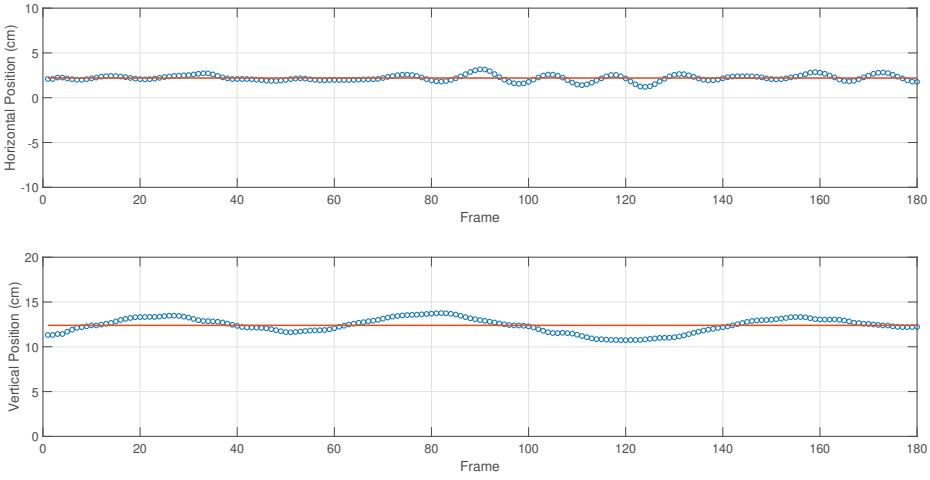

Fig. 10 Representative data for the 5 cm sphere in equilibrium. (Frame rate is 60 fps.)

Figure 11 shows the response of the heavier 3 cm sphere, when supported by the jet on the high setting, to a perturbation induced by poking the sphere with a ruler. The vertical motion exhibits a clear, underdamped oscillation.

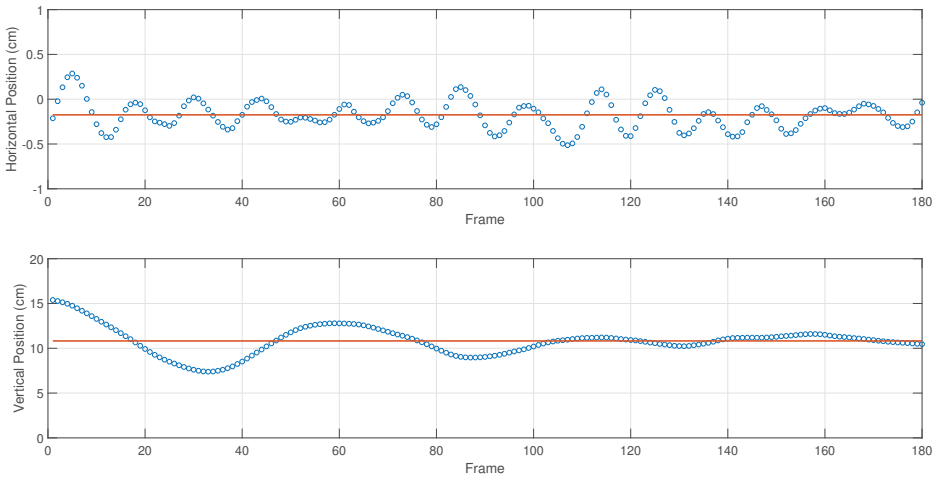

Fig. 11 Representative data for the 3 cm sphere in response to a perturbation. (Frame rate is 60 fps.)

Analyzing the latter portion of the vertical response (lower plot), where the assumption of linear dynamics is less suspect, one finds a natural frequency $\omega_n = 6.9$ rad/s and a damping ratio $\zeta = 0.01$. An oscillation frequency $\omega = 34.3$ rad/s can also be seen in the lateral motion data (upper plot). This lateral oscillation may reflect high frequency wandering of the vertical jet – the frequency is just above the Nyquist frequency for the flow measurements, so it is impossible to know – but it could also represent underdamped lateral oscillations that are excited by random flow perturbations. In that case, ω would represent a damped natural frequency.

Diameter (cm)	Mass (g)	Setting: {L/H}	Avg. Height (cm)
3	1.4	L	10.2
3	2.0	L	5.3
3	2.0	H	9.8
4	2.6	L	2.2
4	2.6	H	8.3
5	2.8	L	3.4
5	2.8	H	13.6

Table 1 Equilibrium heights of four spheres.

To further explore the dynamic modes of motion, we consider analysis similar to that described in Section III.B for a laminar, axisymmetric jet. Using direct measurements of the flow velocity rather than an analytical solution, we may examine predictions about the equilibrium height and key parameter values such as natural frequency and damping ratio.

Doing so, we first note that the Reynolds number based on sphere diameter, over the entire range of diameters and flow speeds, ranges from $10,000$ to $50,000$. Referring to Figure 4, we assume that the drag coefficient is $C_D \approx 0.45$ across all experiments. If we make the much more questionable assumption that the velocity at the sphere's equilibrium height equals the undisturbed velocity at this point, as measured using the Pitot-static probe – that is, if we assume that the sphere has no effect on the surrounding flow velocity – we find a considerable discrepancy between the measured equilibrium height and that predicted by the balance of weight and drag. Clearly the sphere *does* affect the surrounding flow field. The discrepancy between the measured and predicted heights is much lower for the lighter, 3 cm sphere, indicating that the blockage effects are less dramatic in this case. We therefore consider only this case in studying stability. (In all cases, the equilibrium was visibly stable, but the assumptions underlying the stability analysis don't hold in the other cases.)

We consider the stability characteristics for the lighter 3 cm sphere at its equilibrium height of 10.2 cm with the lower hair dryer power setting. Specifically, we compute the natural frequency and damping ratio for vertical and radial motions using the small perturbation model (4), where the components of the gradient and Hessian are computed from flow velocity measurement data.

Doing so, we find a natural frequency of 0.52 rad/s for the vertical motion and a damping ratio of 0.002. These values are both an order of magnitude smaller than that values extracted from data for the small perturbation experiment. That is, the predicted characteristic motion in the vertical direction is an order of magnitude slower and an order of magnitude less damped than that observed in experiments, as seen in the bottom plot of Figure 11. For radial motion, we compute a natural frequency of 0.94 rad/s and a damping ratio of 0.001. This natural frequency corresponds to much slower lateral oscillations than are observed in the top plot of Figure 11.

V. Conclusions

A simple demonstration involving a table tennis ball floating in the vertical flow of a hair dryer illustrates a variety of fundamental concepts involving aerodynamics and rigid body motion. The experiment demonstrates aerodynamic drag, which counteracts the weight of the sphere, and Bernoulli's principle, which helps to explain stability in the radial direction. The demonstration also raises other, more subtle issues such as laminar and turbulent flow and the effect of nonuniform flow on the existence and stability of equilibria. Depending on the available time and resources, and the students' academic level, a secondary STEM educator could use this material to develop a brief introduction or a comprehensive investigation of aerodynamics and stability of motion.

While the qualitative behavior of a heavy sphere in a vertical jet (i.e., the existence of stable equilibria) is captured by a simple, small perturbation model described in the paper, the quantitative agreement with that model is poor. Reasons for the disparity include the significant, unmodeled effect of the sphere on the flow field within the jet and the simple quasisteady aerodynamic model which does not capture time-varying forces associated with vortex shedding.

Acknowledgments

The third author gratefully acknowledges the support of the National Science Foundation under Grant No. IIS-1840044 and the Office of Naval Research under Grant No. N00014-20-1-2621.

References

[1] Feng, J., and Joseph, D. D., "The motion of a solid sphere suspended by a Newtonian or viscoelastic jet," *Journal of Fluid Mechanics*, Vol. 315, 1996, pp. 367–386.

[2] Barois, T., Huck, P. D., Bourgoin, M., and Volk, R., "Equilibrium position of a rigid sphere in a turbulent jet: A problem of elastic reconfiguration," *Physical Review E*, Vol. 96, No. 3, 2017, p. 033105.

[3] Reba, I., "Applications of the Coanda effect," *Scientific American*, Vol. 214, No. 6, 1966, pp. 84–93.

[4] McDonald, K. T., "Levitating beachballs," *American Journal of Physics*, Vol. 68, No. 4, 2000, pp. 388–389.

[5] López-Arias, T., Gratton, L. M., Zendri, G., and Oss, S., "Forces acting on a ball in an air jet," *Physics Education*, Vol. 46, No. 2, 2011, p. 146.

[6] Anderson, J. D., *Introduction to Flight*, 8th ed., McGraw-Hill, New York City, NY, 2015.

[7] Munson, B. R., Young, D. F., and Okiishi, T. H., *Fundamentals of Fluid Mechanics*, John Wiley and Sons, New York City, NY, 1990.

[8] Schetz, J. A., *Injection and Mixing in Turbulent Flow*, American Institute of Aeronautics and Astronautics, New York City, NY, 1980.

[9] White, F. M., *Viscous Fluid Flow*, 2nd ed., McGraw-Hill, New York City, NY, 1991.

[10] Landau, L. D., and Lifshitz, E. M., *Fluid Mechanics*, 2nd ed., Pergamon Press, New York City, NY, 1997.

[11] Batchelor, G. K., *An Introduction to Fluid Dynamics*, Cambridge University Press, Cambridge, U.K., 1967.

[12] de Go Mars, B., "Cd of the smooth sphere as a function of Reynolds number (Reynolds based on the diameter)," , June 2014. Licensed under the Creative Commons BY-SA 3.0 license (https://creativecommons.org/licenses/by-sa/3.0).

[13] Thomasson, P. G., and Woolsey, C. A., "Vehicle motion in currents," *IEEE Journal of Oceanic Engineering*, Vol. 38, No. 2, 2013, pp. 226–242.

[14] Hooper, R., and Young, J., "Media compatibility for IPS PRT pressure sensors," Tech. rep., Freescale Semiconductor, Inc., Tempe, AZ, 2008. Application Note AN3728.

[15] Bose, A., "Track color in video," Tech. rep., Mathworks, October 2016. Downloaded from https://www.mathworks.com/matlabcentral/answers/uploaded_files/44094/track_color_in_video.zip on October 24, 2020.

A. Vertical flow velocity measurements

	r = 0 cm	r = 1 cm	r = 2 cm	r = 3 cm	r = 4 cm	r = 5 cm
z = 2 cm	15.9	12.3	6.9	1.8	1.8	1.7
z = 4 cm	14.2	13.3	5.8	1.9	1.7	1.7
z = 6 cm	14.3	12.1	3.8	1.1	1.9	1.2
z = 8 cm	14.3	12.1	11.7	12.2	5.1	2.0
z = 10 cm	13.8	11.1	12.7	11.1	4.0	2.8
z = 12 cm	13.8	11.1	6.0	1.7	1.6	1.3
z = 14 cm	12.7	9.2	6.4	2.7	1.4	1.2
z = 16 cm	8.2	8.2	5.0	1.7	1.1	1.2
z = 18 cm	9.5	8.3	6.1	4.2	1.6	1.0
z = 20 cm	8.0	5.2	5.8	3.6	0.8	0.0
z = 22 cm	8.6	6.6	3.1	2.9	1.3	0.0
z = 24 cm	7.4	4.4	3.9	3.6	1.1	0.5
z = 26 cm	7.6	4.4	3.9	3.6	1.1	0.5
z = 28 cm	8.1	8.0	4.7	3.2	1.9	0.7
z = 30 cm	4.6	5.1	4.4	2.6	0.7	0.8

Table 2 Average vertical flow velocity w in m/s at "low" setting

	r = 0 cm	r = 1 cm	r = 2 cm	r = 3 cm	r = 4 cm	r = 5 cm
z = 2 cm	17.7	17.1	11.7	2.5	1.7	1.1
z = 4 cm	17.5	15.8	6.6	2.7	2.2	2.4
z = 6 cm	17.5	14.7	8.9	3.0	2.5	2.6
z = 8 cm	17.4	15.3	9.3	2.3	2.4	2.2
z = 10 cm	15.2	12.0	3.9	2.2	1.7	2.0
z = 12 cm	16.5	12.9	8.8	4.0	1.8	1.6
z = 14 cm	14.8	11.2	9.1	3.5	1.7	0.9
z = 16 cm	14.9	13.0	8.0	4.0	1.8	1.6
z = 18 cm	12.7	11.7	7.7	3.6	1.9	1.5
z = 20 cm	11.0	10.0	6.2	3.2	0.0	1.1
z = 22 cm	10.3	6.4	5.5	3.8	2.1	1.7
z = 24 cm	7.0	9.4	6.7	3.6	1.8	1.7
z = 26 cm	10.9	9.3	6.2	5.0	3.0	0.7
z = 28 cm	9.3	8.3	5.5	4.0	1.8	1.0
z = 30 cm	8.4	9.2	5.5	1.4	0.8	2.0

Table 3 Average vertical flow velocity w in m/s at "high" setting